NUMERICAL MODELING OF THE INTERACTION OF A STRONG SHOCK WAVE WITH LIQUID DROPS

V. S. Surov

UDC 533.6.011.72

The paper presents a numerical investigation of the interaction of a strong shock wave (SW) with a drop, or a system of drops, of various liquids. This problem was previously studied by experimental methods mainly [1–5]. Note that there is often a lack of information in a physical experiment. In particular, in experiments on the interaction of SW with drops, their shapes are recorded at different instants but some important characteristics, like pressure and velocity fields, remain undetermined. Moreover, within the scope of a physical experiment it is rather difficult to study the influence of a separate parameter (e.g., liquid viscosity) with the others unchanged (there are no liquids with the density of water and the viscosity of glycerine in nature). A numerical experiment is free from these shortcomings, but we have to use simplified models in that case. In this particular study the gas was assumed to be ideal and the liquid, incompressible and viscous; the breakoff of microparticles from the windward surface of the drop was not taken into account, which reduces the value of the numerical solution but allows us to gain a more penetrating insight into the physics of the processes. The calculations are correct if the influence of the used assumptions is minimal, which impose certain limitations on the range of parameters.

1. Formulation of the Problem and Method of Calculation. Let a plane SW run over a drop at rest in an ideal gas. For a given Mach number of the falling SW ($\mathrm{M} = D/c_0$, D is the propagation velocity of the SW front), the mass velocity of the gas v_s, the density ρ_s, and the pressure p_s behind its front are determined from the expressions

$$\frac{v_s}{c_0} = \frac{\mathrm{M}^2 + \dfrac{p_0}{\rho_0 c_0^2}\left[\sqrt{\left(1 + \dfrac{\rho_0 c_0^2}{p_0}\mathrm{M}^2\right)^2 + æ^2 - 1} - æ\right]}{(æ+1)\mathrm{M}},$$

$$\rho_s = \frac{\rho_0 c_0 \mathrm{M}}{c_0 \mathrm{M} - v_s}, \qquad p_s = p_0 + \rho_0 v_s c_0 \mathrm{M},$$

following from the Rankine–Hugoniot relations. Here $æ$ is the adiabatic index ($æ = 1.4$), c_0 is the sound speed, and the parameters in the undisturbed gas have the subscript 0. According to [6], the liquid is assumed to be viscous and incompressible.

To obtain a numerical solution to the Euler equations, we used Godunov's method and the MAC method [6] for the Navier–Stokes equations. The deformation of a drop was determined by a modification of the method of markers. Since the gas density is significantly less than the liquid density, simplified boundary conditions were used at the contact boundary. The calculation of each time step of the conjugate problem was divided into two stages: first, the "external" problem of a gas flowing around a drop was solved with the contact boundary considered as a movable surface impermeable to the gas; then from the external pressure which was obtained at the first stage the liquid flow was calculated. From the stability conditions, the allowable time step for the gas is 5–10 times less than that for the liquid, so, as a rule, several calculation steps for the gas motion precede one step for the liquid motion. Note that for the strong SW considered here and large

Chelyabinsk State University, Chelyabinsk 454136. Translated from Prikladnaya Mekhanika i Tekhnicheskaya Fizika, Vol. 36, No. 3, pp. 38–44, May–June, 1995. Original article submitted February 8, 1993; revision submitted May 12, 1994.

0021-8944/95/3603-0354$12.50

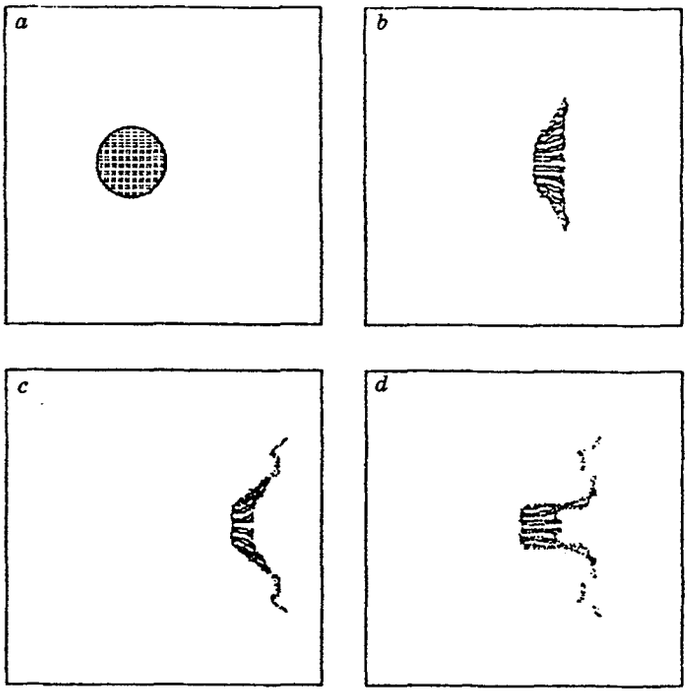

Fig. 1

drops, the surface tension forces are more than an order lower than the aerodynamic forces and, therefore, have no substantial effect on the interaction process.

During the interaction, the deformations of a drop, caused, for example, by generation of thin liquid layers with one of their dimensions less than or equal to the dimensions of one cell, may be so large that the calculation of liquid motion in the layer is impossible by the method in use. In this case (for understanding the process qualitatively) the motion of the elements of the layer was calculated by integrating the differential equations of the motion

$$\Delta m_k \frac{dv_k}{dt} = \Delta p_k S_k,$$

where Δm_k is the mass of a fragment of the liquid layer in the kth cell, v_k is its velocity, and Δp_k is the pressure difference on the opposite sides of the studied fragment of the layer with area S_k.

2. Numerical Results for Single Drops. A series of calculations were made for the interaction of a SW at Mach numbers from M = 3 to M = 10 with spherical drops of water and glycerine ($d_0 = 2$ mm).

Figures 1*a–d* show the positions of the markers which characterize the deformation of the water drop for SW at M = 3 at time 0, 17.8, 30.2, and 37.9 μsec, respectively. As follows from the calculations, at the initial stage the picture of interaction is similar to that of a gas flowing around a solid particle. A detached SW forms ahead of the drop, but its shape and position change with time due to the deformation and acceleration of the drop. By $t = 17$ μsec the drop compresses in the direction of the flow and takes on the form of a lens; then the thinnest (external) part of the drop displaces from its base core and forms a "hat" brim (in terms of [5]). The second local maximum of pressure appears near the base of the "hat" brim (the first one is near the symmetry axis ahead of the drop). The existence of the second local maximum leads to the essential reorganization of the liquid flow within the drop. In particular, when the pressure increases, the direction of motion of the liquid particles near the base of the "hat" brim changes, being displaced toward the symmetry axis, which results in compressing the liquid within the drop core up to the axis (Fig. 1*d*). This is how the liquid jet is generated, as opposed to the flow observed in experiments [5].

Figure 2 presents the dependence of the relative enlargement of the water drop $\Delta d/d_0$ (solid line) on

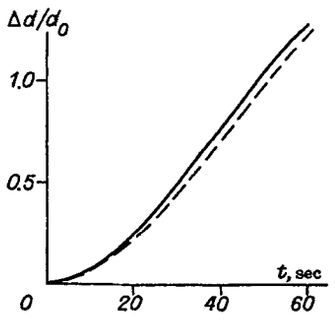

Fig. 2

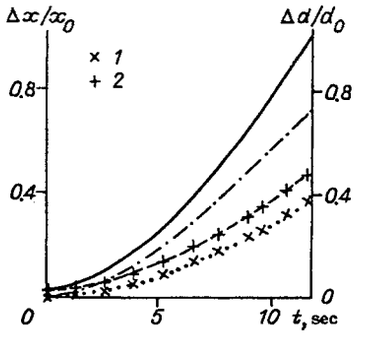

Fig. 3

time t, and the dashed line is the same dependence for a drop with the density of water and the viscosity of glycerine. Thus, an increase in viscosity (about 1000 times) leads to a slightly decreased growth of the drop's transverse dimension. As the Mach number of the falling SW increases, the influence of the liquid viscosity becomes weaker, as seen in Fig. 3 which shows the time dependences of the relative change in the transverse dimension of a glycerine drop (dotted line) and a drop with the density of glycerine and the viscosity of water (points *1*) for a SW at M = 10. Figure 3 also presents the dependences of the relative displacement $\Delta x/x_0$ for these drops (the dashed curve and points *2*, respectively). The deformation velocity of the drop and its displacement substantially depend on the liquid density, as seen in Fig. 3 which presents the corresponding data for a water drop (M = 10) where the solid curve shows the dependence of the relative change in the drop's transverse dimension, and the dot-and-dash curve marks its relative displacement.

Note that in calculations of the interaction of a SW (M = 3) with a glycerine drop we can see that the "hat" brim tears away from the core and therefore has no substantial influence on the drop's core destruction, which is of "parachute" type. The calculated deformation of the glycerine drop is also in agreement with experiments [5].

Thus the assumptions used here, relative both to the mathematical model and to the calculation method, do not grossly distort the general picture of the process of drop deformation and are acceptable for the investigated range of interaction velocities.

3. Calculation Results for a Drop Screen. The problem considered here is the problem of the interaction of a plane SW falling normally on a drop screen which is an ensemble of large ($d \sim 1$ mm) liquid drops uniformly distributed over a plane. Screens of very small porosity were not considered in the work since in the literature this problem has been investigated rather completely within the scope of the model of mutually penetrating continuums [7, 8]. The data presented below were calculated for a SW at M = 10 which interacts with a screen irregular in thickness and porosity for the "staggered" disposition of water drops of the same size in a layer. For a screen consisting of glycerine drops, the calculation results are qualitatively similar; in this case the velocities of motion of the drop and the degree of their deformation appear to be somewhat lower than for the water screen. The diameter of water drops varied from 1 to 2.5 mm. The nature of the interaction depends essentially on the porosity of the drop layer (parameter K), which is determined via the relation of the volume of pores to the whole screen volume, on layer's thickness, and on the mutual disposition of particles in the layer. Note that due to the symmetric disposition of particles the resulting flow is also symmetric, which allows us to reduce the calculation region significantly and to study not the whole screen but only a part of it.

Figure 4*a* presents the positions of drops calculated by $t = 23.8$ μsec after interaction of SW with the screen which consists of ten layers of water drops 1.4 mm in diameter ($K = 0.83$). Figure 4*b* shows the diagrams for distribution of the pressure $P = p/(\rho_s u_s^2)$ (solid curve) and the velocity component u_x (dashed curve) in relation to a linear coordinate which is directed transversely to the drop layer through the particles'

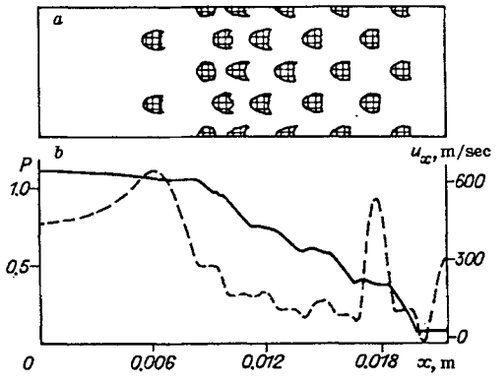

Fig. 4

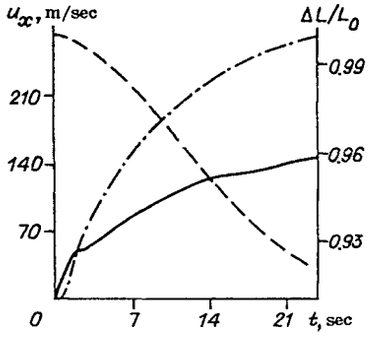

Fig. 5

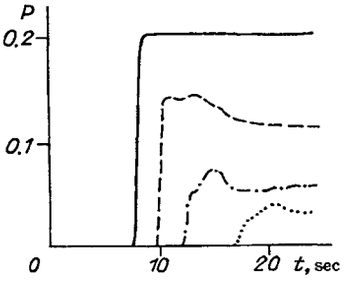

Fig. 6

centers calculated at $t = 23.8$ μsec (the point with $x = 0$ coorresponds to the extreme left boundary of the region in Fig. 4*a*). Figure 5 presents the dependences of the velocities of the first (solid curve) and the second (dot-and-dash curve) drop layer, and the dependence of the relative screen thickness $\Delta L/L_0$ (dashed curve) on time t.

On analyzing the numerical results, we can present the physical picture of the interaction as follows. As the falling SW approaches the screen, a reflected SW forms. Its velocity, and to a smaller degree its amplitude, depend on the screen thickness and porosity. A compression wave propagates through the drop layer. Its propagation velocity is significantly less than the velocity of the falling SW, so a time delay is observed in the passage of SW through the screen. This is seen from Fig. 6 which shows the pressure curves at a point near the boundary of the calculated region behind the screen as functions of time t. Dashed and dot-and-dash lines correspond to the screens of the same porosity $K = 0.83$ but consisting of four and ten drop layers respectively; the dashed line is the dependence of pressure for a screen of ten drop layers and a porosity $K = 0.72$, the solid line is the pressure in the absence of a screen.

As the compression wave reaches the back screen's surface, the SW propagates to the right of the layer. The pressure within the layer stabilizes and takes the form of a stepwise dependence, with its maximum value fixed near the "left" screen's boundary and its minimum value at the opposite side (Fig. 4*b*). Since the pressure distribution over the drop layer is nonuniform, the velocity of motion of the drop in the layers is also nonuniform: maximum is with the second layer drops (at the first moment of interaction it is with the the first layer of particles), minimum is with the particles at the "right" boundary, which results in the screen thickening on the side of the falling SW (Fig. 4*a* and 5). The first drop layer is separated from the others

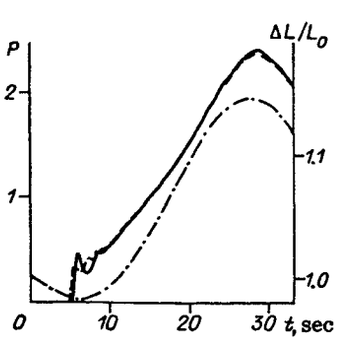

Fig. 7

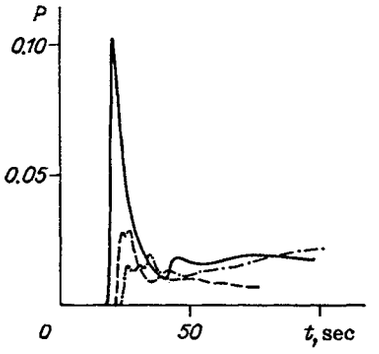

Fig. 8

since the pressure gradient decreases near the first layer's drops because of interaction with the SW reflected from the second layer of particles.

Thereafter the velocities of the drop motion in the screen level off at the cost of interaction of the "faster" drops with particles of subsequent layers, hence their resulting velocity decreases. The decrease in the amplitude of the passed SW depends on the screen's thickness and porosity (Fig. 6). Thus, for a ten-layer screen [$K = 0.72$ (0.83)] the amplitude of the passed SW is reduced 7 (3.7) times with respect to the falling SW. For a four-layer screen ($K = 0.83$) the amplitude of the passed SW is reduced 1.8 times. As the velocity of the particles increases, the pressure in the reflected SW decreases slowly. The increase in the velocity of particles in the layer will continue untill the pressure to the left and to the right of the screen equalizes.

Thus, the presence of a drop screen along the path of the SW leads to a time delay in passage of the SW through the layer, which is connected with a decrease in the velocity of the compression wave propagation within the layer; the delay is longer the greater the screen's thickness and the smaller its porosity. The amplitude and specific momentum of the SW that passed through the drop layer decrease. By interacting with the SW, the screen shrinks. Since we are dealing with a plane problem, there are no significant transverse pressure gradients in the neighborhood of the drops, hence the drops, in contrast to spherical ones, experience mainly a shear (longitudinal) deformation (Fig. 4*a*).

The presence of a solid wall behind the screen changes the nature of interaction. We observe a difference after reflection of the SW from an obstacle. Given below are the calculated data for a drop screen consisting of four layers of water drops 1.4 mm in diameter. Figure 7 presents the pressure curves ahead of an obstacle on a symmetry plane (solid curve) and on a plane through the center of the first layer of particles (dashed curve); the dot-and-dash line shows the screen's relative thickness as a function of time. The calculations show that the pressure along an obstacle levels off rather quickly. The velocity of particles in the screen increases until the pressure to the left and to the right of the screen levels off, the screen's porosity being decreased (except for the first layer which is remote from the subsequent ones). Because of the inertness of the particles which, while slowing down, continue to move toward the obstacle and are carrying along the surrounding gas, the pressure behind the screen increases further. At this stage the behavior of the screen is similar to that of a piston which compresses a gas ahead of an obstacle. Thus, after some instant the pressure behind the screen is higher (more than 1.5 times) than that in the reflected SW without a screen (Figs. 6, 7). Later on, the gas begins flowing from the increased pressure region between the screen and the wall to the lower pressure region (in front of the screen). This regime of flow is adhered to for a sufficiently long time until the impact of particles on an obstacle.

Note that if a drop screen has a layer which consists, for example, of larger drops and has permeability less than that of the other layers, then separation of the screen is observed in the layer's disposition. But further the velocities of motion of the drop in the screen level off because of the impact of "faster" drops on the subsequent layers' particles. Similar processes take place in other cases also, for example, in breaking the

symmetry of disposition of drops in the screen.

The shock waves considered above are "long" shock waves which have a pressure profile in the form of a half-infinite "step." In the explosion of a charge the pressure profile is "triangular." Assume that at $t = 0$ the increased pressure zone with parameters $p = 0.118 \cdot 10^8$ Pa, $\rho = 7.7$ kg/m^3, $u = 0$ is disposed in the cells of the calculation region from $x = 1$ to $x = 2$ (outside this region the gas is at atmosphere conditions). When $t > 0$, shock waves propagate to the right and to the left of the increased pressure region. If there is a drop screen along the path of the SW, then it should decay. This is evident from Fig. 8 which presents the pressure curves at a point ahead of an obstacle behind the screen as functions of time t. Dashed and dot-and-dash lines correspond to screens of porosity $K = 0.83$ and 0.72, respectively (in all cases the screen consists of four water drop layers); the solid line is the dependence of pressure in the absence of a screen. It is seen from the data presented above that in the presence of the screen the maximum (peak) pressures decrease substantially; moreover, the current values of pressure in front of an obstacle decrease in the case of a screen of relatively small porosity. However, for a screen of porosity $K = 0.72$ the pressure in front of an obstacle exceeds the pressure level without the screen (since $t = 80$ μsec), which is accounted for by the "piston" effect.

In conclusion, the author is grateful to Prof. V. M. Fomin and Prof. B. V. Litvinov for formulation of the problems and useful discussion of the results.

REFERENCES

1. W. G. Reinecke and G. D. Waldman, "An investigation of water drop disintegration in the region behind strong shock waves," Proc. 3rd Intern. Conf. Rain Erosion and Related Phenomena, Hartley–Whitney, Hampshere (1970).
2. A. A. Buzukov, "Disintegration of drops and jets with an air shock wave," Prikl. Mekh. Tekh. Fiz., No. 2 (1963).
3. B. E. Gel'fand, S. A. Gubin, and S. M. Kogarko, "Differences in drop breakup in shock waves and their characteristics," Inzh. Fiz. Zh., **27**, No. 1 (1974).
4. B. M. Belen'kii and G. A. Evseev, "Experimental investigation of drop disintegration from gas motion behind a shock wave," Izv. Akad. Nauk SSSR, Mekh. Zhidk. Gaza, No. 2 (1974).
5. V. M. Boiko, A. N. Papyrin, and S. V. Poplavskii, "Dynamics of droplet breakup in shock waves," Prikl. Mekh. Tekh. Fiz., No. 2 (1987).
6. V. S. Surov and V. M. Fomin, "Numerical modeling of interaction of a water drop with a strong air shock wave," Prikl. Mekh. Tekh. Fiz., **34**, No. 1 (1993).
7. A. I. Ivandaev and A. G. Kutushev, "Influence of screening gas–suspension layers on shock wave reflection," Prikl. Mekh. Tekh. Fiz., No. 1 (1985).
8. B. S. Kruglikov and A. G. Kutushev, "Shock wave decay with screening lattices," Fiz. Goreniya Vzryva, **24**, No. 1 (1988).